PHYSICAL REVIEW B VOLUME 57, NUMBER 14 1 APRIL 1998-II

Dimensional-crossover behavior in randomly layered media

Man-Chung Chan, Zhao-Qing Zhang, and Po-Wan Woo
Department of Physics, Hong Kong University of Science and Technology, Clear Water Bay, Kowloon, Hong Kong, China
(Received 20 October 1997)

We study the lateral transport of two-dimensional randomly layered media in the presence of isotropic randomness. The hopping anisotropy is also included. Equilibration length and channel occupation number are calculated by using both the recursive Green's-function method and the rate-equation approach. Our results show clearly a transition from ergodic to nonergodic transport as the number of layers increases. This describes a dimensional-crossover behavior from two-dimensional-like anisotropic hopping systems to one-dimensional-like randomly layered media. [S0163-1829(98)52114-5]

The study of transport and localization properties of randomly layered media with isotropic randomness (RLMIR) has been a challenging task due to the presence of both layer randomness and isotropic randomness. However, their interplay has been shown to give rise to many transport phenomena not seen in other disordered systems.[1–3] Physical examples of RLMIR are the Earth's subsurface and random superlattices with lateral inhomogeneities. The layer randomness makes transport in such systems anisotropic. Previous calculations on three-dimensional (3D) systems have indicated that, when the ratio of the strength of layer randomness to that of isotropic randomness is larger than a certain critical value, the system is 1D-like and all states are localized.[1] Also, in the previous studies of lateral transport on 2D systems, it has been found that the transport is nonergodic in channel space due to the existence of a dominant channel.[2,3] As a function of propagating channels M_c, it has also been found that the averaged number of occupied channels exhibits a finite-size scaling behavior that is intermediate between 1D and 2D, i.e., $\langle N_{\rm oc}\rangle \approx \sqrt{M_c}$.[2] All these transport behaviors suggest that RLMIR is different in nature from other disordered systems, including anisotropic hopping systems (AHS) where the anisotropy arises purely from the hopping integrals.[4] For AHS, it has been shown that Anderson localization transition occurs in 3D independent of the anisotropy and the isotropic transport behaviors can be recovered after some proper rescaling of lengths in different directions.[4] Thus, we have two types of anisotropic systems with entirely different transport properties.

There are two important questions we would like to address in this work. Firstly, we cannot exclude the possibility that the behavior $\langle N_{\rm oc}\rangle \approx \sqrt{M_c}$ found in Ref. 2 describes only a crossover behavior due to the small number of propagating channels, i.e., $\max\{M_c \approx 25\}$, involved in the calculations.[2] If this is the case, what is the true property of the 2D RLMIR? Secondly, does there exist any connections between RLMIR and AHS and what is the crossover behavior between these two types of anisotropic systems? In order to answer these questions, we consider a system which has both layer randomness and hopping anisotropy. Such a system can possess a maximum number of propagating channels, i.e., $\max\{M_c\}$ =number of layers, and enables us to study the crossover between RLMIR and AHS. We use the following tight-binding Hamiltonian to describe the RLMIR:

$$H=\sum_{\alpha} \varepsilon_{\alpha} a_{\alpha}^{\dagger} a_{\alpha} + \sum_{[\alpha,\beta]} t_{\alpha\beta} a_{\alpha}^{\dagger} a_{\beta}, \tag{1}$$

where α,β are site indices, and $[\alpha,\beta]$ indicates α and β are nearest neighbors. The lattice constant is set to be unity. We assume that the nearest-neighbor hopping integrals are different in different directions. For a 2D system, we choose the z axis as the layering direction and the x axis as the lateral direction. For convenience, we set $t_x=1$ as the energy scale and have chosen $t_z \ll t_x$ in our calculations. The site energy ε_{α} consists of two parts:

$$\varepsilon_{\alpha}=\eta_z+\delta_{\alpha}. \tag{2}$$

η_z describes the layer energy and is a constant for all sites lying in a given layer at fixed z, but varies randomly as z varies with a flat distribution of width W_1. δ_{α} is a random number that varies independently from site to site with a flat distribution W. W_1 and W measure the strengths of layer randomness and isotropic randomness, respectively. The AHS is recovered when $W_1=0$. In the presence of W_1, all states are localized along the z direction. These localized wave functions act as overlapped channels for the propagation of waves along the x direction. For any particular layer configuration of a N-layer system, i.e., a given set of $\{\eta_z\}$ for $z=1,2,\ldots,N$, one can solve the 1D eigenvalue problem along the z direction and obtain a set of N eigenfunctions $\varphi_n(z)$ and eigenvalues E_n. The wave energy can be written as $E=E_n+2\cos k_n$, where k_n is the wave vector of the nth channel for the propagation along the x direction. When $|E-E_n|>2$, k_n is imaginary and the channel is denoted ''evanescent.'' When $|E-E_n|<2$ and k_n is real, the channel is denoted ''propagating.'' The Fermi-energy E is set to be 0 in our calculations. In the previous 2D study with $t_x=t_z=1$, strongly localized channel functions were produced by using a large W_1 ($W_1=15$). This made most of the channels nonpropagating and severely limited the study of lateral transport to a small number of propagating channels. This difficulty is overcome by choosing $t_z \ll t_x$. Since the localization length of $\varphi_n(z)$ scales with $-1/\ln(t_z)$, strongly localized channel wave functions can be achieved with $t_z \ll 1$ even when $W_1 \leqslant 1$. Thus, we can have all channels propagating in the x direction. In this case the strength of layer randomness is measured by the dimensionless ratio W_1/t_z.

In this work, we study the finite-size scaling behavior of the averaged occupied channels $\langle N_{\rm oc}\rangle$ at various ratios of W_1/t_z by using both the recursive Green's-function (RGF) method[5] and the classical rate equation (CRE) approach.[3] In the RGF calculations, we connect the disordered sample of length L, where $W\neq 0$, to two pure leads on both sides of the sample. These leads have the same layer configuration and anisotropy in t_x and t_z but $W=0$. The transmission amplitudes t_{nm} with incoming wave at the mth channel and outgoing wave at the nth channel form a $N\times N$ matrix and can be calculated numerically using the RGF method.[5] In our calculations, a periodic boundary condition is used in the z direction. It has been shown analytically that when sample length L is larger than some equilibration length, $L_{\rm eq}$, t_{nm} has the asymptotic form

$$t_{nm}(L)\cong 2\exp(-\lambda_1 L)a_{1,n}(L)g_1^*(m),$$

where $1/\lambda_1$ is the localization length of the system and $g_1(m)$ is the normalized eigenvector of t^+t corresponding to the largest eigenvalue $2/\cosh(2\lambda_1 L)$.[3,6] The normalized vector $a_{1,n}(L)$ is related to $g_1(m)$ by a unitary transformation arising from the isotropic scattering. For each chosen layer configuration, $g_1(m)$ depends only on the configuration of isotropic randomness [δ_α in Eq. (2)] in the region $0<L<L_{\rm eq}$ and becomes a fixed vector when $L>L_{\rm eq}$. Therefore, the value of $L_{\rm eq}$ can be determined from the length where the ratios $t_{nm}(L)/t_{n\ell}(L)\cong g_1^*(m)/g_1^*(\ell)$ become L independent. From this relation we can obtain the relative occupation probability in the nth outgoing channel as $\theta_n(L)=|t_{nm}(L)|^2/\Sigma_{n=1}^N|t_{nm}(L)|^2\cong|a_{1,n}(L)|^2$, which is independent of the incoming channel m.[3] In this asymptotic region, the statistics of $\theta_n(L)$ are stationary and the relative channel occupation distribution can be obtained by taking the average in L, i.e., $\overline{\theta_n}\equiv\langle\theta_n(L)\rangle_{L>L_{\rm eq}}$. The average number of occupied channels is defined as $N_{\rm oc}=1/(\Sigma_n\overline{\theta_n^2})$.[2] For AHS, it is expected that all the channels are evenly distributed and $N_{\rm oc}\cong N$. This ergodic property makes the AHS in the same universality class as the other isotropic systems, whereas for the RLMIR, the distribution of channels is not ergodic.[2,3] In particular, if the system is 1D-like, we would expect that $N_{\rm oc}$ approaches a constant value in the large N limit.

For a given layer configuration $\{\eta_z\}$, the statistics of θ_n can be obtained by the following two equivalent sampling procedures: (I) sampling at different $L>L_{\rm eq}$ in a single configuration of $\{\delta_\alpha\}$ in Eq. (2), and (II) sampling at a fixed $L>L_{\rm eq}$ with different configurations of $\{\delta_\alpha\}$. For all the calculations discussed below, we have set $W=1$ and $t_z=0.01$. The equivalence of the two sampling procedures can be demonstrated by the following example. We consider a three-layer system with layer energies, $\eta_1=0$, $\eta_2=1.5$, and $\eta_3=-0.5$. The corresponding channel energies are $E_1=0.000\,13$, $E_2=1.500\,12$, and $E_3=-0.500\,25$, with $n=1$ as the dominant channel. The distribution function of θ_1/θ_2 obtained from procedures (I) and (II) is plotted in Fig. 1 in solid circles and triangles, respectively, in logarithmic scale. Similarly, the distribution function of θ_3/θ_1 is plotted in open circles and triangles for procedures (I) and (II), respectively. In each sampling, 6000 data points were collected. The equivalence of two sampling procedures is evident.

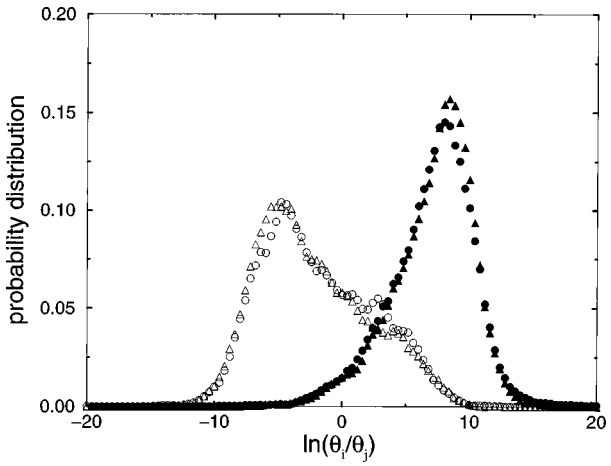

FIG. 1. At $W=1$ and $t_z=0.01$ with channel energies $E_1=0.000\,13$, $E_2=1.500\,12$, and $E_3=-0.500\,25$, the distributions of $\ln(\theta_1/\theta_2)$ and $\ln(\theta_3/\theta_1)$ are plotted in solid and open symbols, respectively. The ''circles'' and ''triangles'' denote the results of sampling procedure (I) and (II), respectively.

For RLMIR with a given layer number N and layer randomness W_1, we have to take a configurational average of $N_{\rm oc}$ over many different layer configurations. The averaged value $\langle N_{\rm oc}\rangle$ is then calculated as a function of N. In order to cover from strong to weak layer randomness, we have chosen $W_1=1$, 0.1, and 0.01, or $W_1/t_z=100$, 10, and 1. For each case the values of N we have studied are $N=2^M$ with $M=1,2,\ldots,$ and 7. For $W_1=0.1$ and 0.01, the sampling procedure (I) was used. The relative channel occupation distribution is averaged in L from $L_{\rm eq}$ to $L_{\rm eq}+5000$. The number of layer configurations ranges from 1000 to 50 with increasing N. For the case of strong layer randomness $W_1=1$, sampling procedure (I) becomes less effective due to weak channel hoppings and procedure (II) was adopted. The layer configuration ranges from 500 to 50. At each layer configuration, five configurational averages for the isotropic randomness were performed. The results of our calculations are shown in Fig. 2 in solid triangles, diamonds, and circles for $W_1=1$, 0.1, and 0.01, respectively. The standard deviations are also shown if their values are greater than the symbol size. For the case of strong layer randomness $W_1=1$, $\langle N_{\rm oc}\rangle$ saturates to the value 5 when the number of layers is greater than 16. Similar is the case of $W_1=0.1$. However, the saturation value of $\langle N_{\rm oc}\rangle$ ($\cong 21$) and the crossover width N_c ($\cong 32$) both became larger. In the AHS limit when W_1/t_z becomes small, both values will diverge as indicated in the case of $W_1=0.01$. These results show clearly that the RLMIR is 1D-like in the large N limit. In fact, for any layer randomness W_1/t_z, there always exists a crossover width N_c, below which the lateral transport is ergodic and above which it becomes nonergodic. Thus the AHS (or other isotropic random systems) is unstable against any layer randomness. It will crossover to the RLMIR when the number of layers becomes large. These results give the definitive answers to the questions addressed in this work.

The crossover from the ergodic to nonergodic regime is more transparent in the distribution function of the averaged

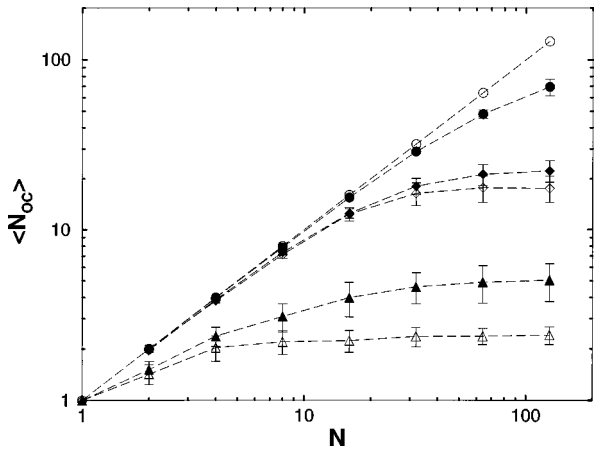

FIG. 2. At $W=1$ and $t_z=0.01$, the average number of occupied channels is plotted as a function of sample width N for the cases of $W_1=1$ (triangles), 0.1 (diamonds), and 0.01 (circles). The solid and open circles denote the results of recursive Green's-function and rate equation calculations, respectively.

occupied channels $P_N(N_{oc})$. In Fig. 3, we plot (in solid symbols) $P_N(N_{oc})$ for the cases of $W_1=0.1$, $N=4$, 8, and 16 in circles, triangles, and diamonds, respectively. For this case of $N=4$, the distribution is peaked at $N_{oc}=4$. This implies that the system is in the ergodic regime. With increasing N, the peak position is shifted towards a lower value than $N_{oc}=N$ together with a larger variance. The nonergodic regime is reached when $N>N_c\approx 32$. In this regime, $P_N(N_{oc})$ seems to saturate to a fixed distribution independent of N. This is shown in the inset of Fig. 3, where $P_N(N_{oc})$ is plotted for the case of $N=32$ and 64 in solid inverse triangles and squares, respectively. In Fig. 4, we plot the probability distribution of L_{eq}, $P_E(L_{eq})$, for the case of $W_1=0.1$, $N=4$, 8, and 16 in circles, triangles, and diamonds, respectively (all solid symbols). These functions can be described by an inverse gamma function of the form

$$P_E(L_{eq})=[\beta^{\alpha}/\Gamma(\alpha)]L_{eq}^{-\alpha-1}\exp(-\beta/L_{eq})$$

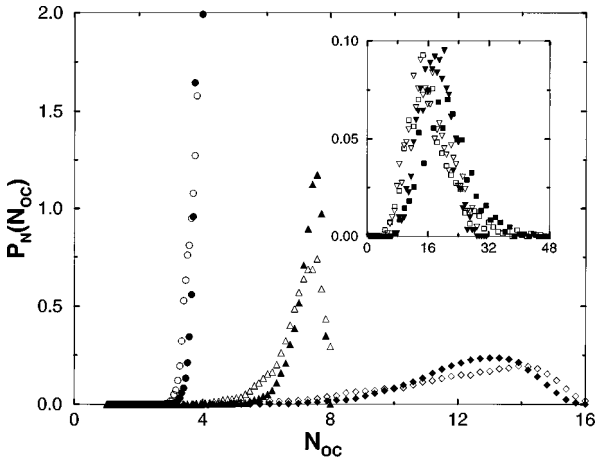

FIG. 3. At $W=1$, $W_1=0.1$, and $t_z=0.01$, the distribution function of the number of occupied channels is plotted for the sample width $N=4$ (circles), 8 (triangles), and 16 (diamonds). The cases of $N=32$ (inverse triangles) and $N=64$ (squares) are shown in the inset. The solid and open circles denote the results of recursive Green's-function and rate equation calculations, respectively.

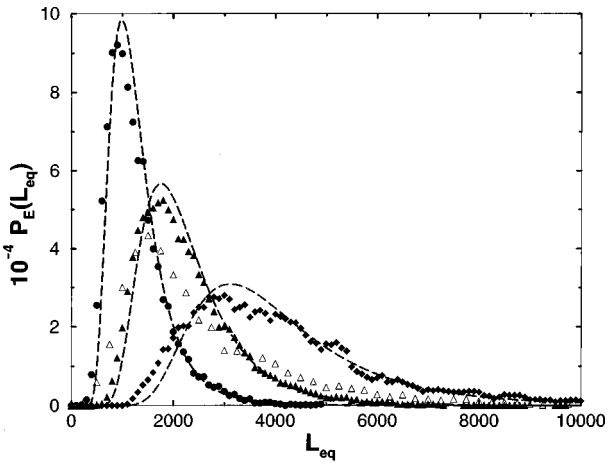

FIG. 4. At $W=1$, $W_1=0.1$, and $t_z=0.01$, the distribution function of the equilibration length L_{eq} is plotted for the sample width $N=4$ (circles), 8 (triangles), and 16 (diamonds). The solid and open circles denote the results of recursive Green's-function and rate equation calculations, respectively.

as shown by the dashed curves.[7] The values of β varies from 7423 to 44 086, whereas the decay exponent α is within 7.0 ± 0.2 insensitivity to the parameters W_1 and N. The variance of this distribution function also increases with N. However, we do not see the sign of saturation in this case. This is expected because it takes longer for a channel far away from the dominant channel to reach equilibrium. Thus, for a sample of fixed L, the lateral transport is determined mainly by the transport in the transient region when N becomes large so that $L<L_{eq}$. In this region, other eigenvectors of $t^{\dagger}t$ become important.

We have also studied this problem independently by using the classical rate equation (CRE) approach, which was proposed to describe the lateral transport in the limit of strong layer randomness.[3] Its validity has been demonstrated in a quantitative way for the case of two channels.[3] Here, we apply it to many-channel systems. In this approach, the Hamiltonian of Eqs. (1) and (2) are written in the channel representation using E_n and φ_n. The isotropic randomness gives rise to both the localization of each channel and the hopping among channels. Due to the small overlap between two channels, the hopping among channels can be treated incoherently. Therefore, the probability $P_n(L)$ of occupying the nth channel at distance L from the injection point satisfies the following equations

$$\frac{dP_n}{dL}=\sum_{m\neq n}^{N}(w_{nm}P_m-w_{mn}P_n)-\frac{2P_n}{\xi_n}, \tag{3}$$

where, w_{nm} is the channel hopping rate, describing the probability of hopping from channel m to n per unit sample length. From the Born approximation, the hopping rate can be written as

$$w_{nm}=\frac{\pi W^2}{6\nu_m}\rho_{1D}(E-E_n)\sum_z|\varphi_n(z)\varphi_m(z)|^2, \tag{4}$$

where ν_m is the wave velocity of channel m, i.e., $\nu_m=[4-(E-E_m)^2]^{1/2}$, and $\rho_{1D}(E-E_n)=1/(\pi\nu_n)$ is the 1D density of state per site.[8] The 1D localization length ξ_n of the

nth channel is determined by the channel energy E_n and the effective randomness $W_n = W(\Sigma_z |\varphi_n(z)|^4)^{1/2}$ and can be calculated by using the standard transfer-matrix method.[9]

The solution of Eq. (3) has the form $P_n(L) = \Sigma_i a_i V_i(n) \exp(-\gamma_i L)$, where γ_i represents the ith eigenvalue of the matrix $-q_{nm} = -w_{nm} + (\Sigma_{l \neq n} w_{ln} + 2/\xi_n)\delta_{nm}$ on the right-hand side of Eq. (3). $V_i(n)$ is the corresponding normalized eigenvector with $\Sigma_n V_i(n) = 1$. The coefficient a_i's are determined by the initial condition $P_n(0)$. For a single injection channel m, we have $P_n(0) = \delta_{nm}$. In the large L limit, $P_n(L)$ is dominated by the term with the longest decay length, say $1/\gamma_1$, and the eigenvector $V_1(n)$ determines the asymptotic channel occupation ratios, i.e., $P_n/P_m = V_1(n)/V_1(m)$, which are independent of initial condition. This ratio is equivalent to θ_n/θ_m in the RGF method. The equilibration length $L_{\rm eq}$ can be determined from the condition that $P_n(L_{\rm eq})/P_m(L_{\rm eq}) \cong V_1(n)/V_1(m)$ for all possible injection channels. The number of occupied channels becomes $N_{oc} = 1/[\Sigma_n V_1^2(n)]$.

In the limit of $t_z \ll 1$, by using perturbation theory, it can be shown that the equilibration length for the mth injection channel has the form $L_{\rm eq}(m) \approx -(\alpha_m - \alpha_1)^{-1} \ln[w_{m1} w_{1m}/(\alpha_m - \alpha_1)^2]$, where $\alpha_i \equiv 2/\xi_i$. If we use l_{m1} to denote the separation between channels m and 1 and the asymptotic properties of $\alpha_m, \alpha_1 \propto W^2$ and $w_{m1} = w_{1m} \propto W^2 t_z^{2l_{m1}}$, we have $L_{\rm eq}(m) \approx -[4l_{m1}/(\alpha_m - \alpha_1)] \ln t_z + C$, where C is independent of t_z. Thus, $L_{\rm eq}$ is determined by the largest value of $L_{\rm eq}(m)$ for all m greater than 1. In the case of the three-layer system discussed earlier, we found $L_{\rm eq} \approx -1008 \ln t_z + 2266$. This analytic result agrees well with the result of RGF calculations, which gives $L_{\rm eq} \approx -1046 \ln t_z + 2211$ for $t_z < 0.01$. This result exhibits an inverse proportionality between the equilibration length and the localization of channel wave functions in the regime of strong layer randomness. Also, from the dominant eigenvector V_1, we found $\ln[V_1(1)/V_1(2)] = 8.5$ and $\ln[V_1(3)/V_1(1)] = -4.8$. These values are close to the peak positions of 8.2 and -4.9 in the distribution of $\ln(\theta_1/\theta_2)$ and $\ln(\theta_3/\theta_1)$ shown in Fig. 1, respectively.

In the study of finite-size scaling, we have repeated all the calculations carried out by the RGF method. We have performed 2000 to 500 layer configurations with increasing N. The results of $\langle N_{\rm oc} \rangle$ are shown in Fig. 2 by open symbols in triangles, diamonds, and circles for the cases of $W_1 = 1$, 0.1, and 0.01, respectively. For the cases of $W_1 = 1$ and 0.1, crossover from ergodic to nonergodic regime are also evident. In the case of weak layer randomness, $W_1 = 0.01$, large overlaps between channel wave function make CRE invalid. As a result, it overestimates the value of $N_{\rm oc}$. Therefore, we do not see the crossover occur even when $N = 128$. The distribution function for $N_{\rm oc}$ is plotted by open symbols in Fig. 3 for the case of $W_1 = 0.1$ and $N = 4$ (circles), 8 (triangles) and 16 (diamonds), $N = 32$ (inverse triangles) and 64 (squares). The last two are shown in the inset. The distribution of $L_{\rm eq}$ is shown in Fig. 4 in open triangles for the case of $W_1 = 0.1$ and $N = 8$. All these distribution functions agree with the results of RGF calculations.

In summary, from both RGF and CRE calculations, we have demonstrated clearly a crossover from ergodic to nonergodic transport in RLMIR. The AHS is unstable against the introduction of layer randomness. A dimensional crossover from 2D-like to 1D-like transport will occur when the number of layers becomes large.

The authors thank P. Sheng for discussions. We also wish to acknowledge the support of Hong Kong RGC Grant No. HKUST 686/96P.

[1] W. Xue, P. Sheng, Q. J. Chu, and Z. Q. Zhang, Phys. Rev. Lett. **63**, 2837 (1989); Z. Q. Zhang, Q. J. Chu, W. Xue, and P. Sheng, Phys. Rev. B **42**, 4613 (1990); Q. J. Chu and Z. Q. Zhang, *ibid.* **48**, 10 761 (1993).

[2] P. Sheng and Z. Q. Zhang, Phys. Rev. Lett. **74**, 1343 (1995).

[3] Z. Q. Zhang and K. C. O, Phys. Rev. B **53**, R11 917 (1996).

[4] W. Apel and T. M. Rice, J. Phys. C **16**, L1151 (1983); Q. Li, C. M. Souloulis, E. N. Economou, and G. S. Grest, Phys. Rev. B **40**, 2825 (1989); I. Zambetaki, Q. Li, E. N. Economou, and C. M. Soukoulis, Phys. Rev. Lett. **76**, 3614 (1996).

[5] P. A. Lee and D. Fisher, Phys. Rev. Lett. **47**, 882 (1981).

[6] A. D. Stone, P. A. Mello, K. A. Muttalib, and J. L. Pichard, in *Mesoscopic Phenomena in Solids*, edited by B. L. Altshuler, P. A. Lee, and R. A. Webb (North-Holland, Amsterdam, 1991).

[7] For instance, M. A. Tanner, *Tools for Statistical Inference: Methods for the Exploration of Posterior Distributions and Likelihood Functions* (Springer, New York, 1996).

[8] P. Sheng, *Introduction to Wave Scattering, Localization, and Mesoscopic Phenomena* (Academic, New York, 1995).

[9] A. Mackinnon and B. Kramer, Z. Phys. B **53**, 1 (1983).